

Suzaku Observation of the Radio Halo Cluster Abell 2319: Hard X-ray Properties and Gas Dynamics

Motokazu Takizawa¹, Chika Sugawara¹, and Kazuhiro Nakazawa²
¹Yamagata University, ²University of Tokyo

(Abstract)

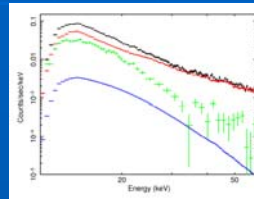
We present the results of Suzaku observation of the radio halo cluster Abell 2319. The metal abundance in the central cool region is found to be higher than the surrounding region, which was not resolved in the former studies. We find for the first time that the line-of-sight velocities of the intracluster medium in the observed region are clearly different than that of A2319B subgroup, though any velocity difference within the region is not detected. Hard X-ray emission from the cluster is clearly detected, but its spectrum is likely thermal. Although the results slightly depend on the detailed spectral modeling, it is robust that the upper limit of the power-law component flux and lower limit of the magnetic field strength become $\sim 3 \times 10^{-11}$ erg s⁻¹ cm⁻² and ~ 0.2 μ G, respectively. Considering the lack of a significant amount of very hot (~ 20 keV) gas and the strong bulk flow motion, it is more likely that the relativistic non-thermal electrons responsible for the radio halo are accelerated through the intracluster turbulence rather than the shocks.

Introduction

Diffuse non-thermal synchrotron radio emission is found in a significant fraction of galaxy clusters, which indicates that there exist both the relativistic electrons and magnetic field as well as the thermal intracluster medium (ICM) in the intracluster space. Although the origin of these non-thermal electrons is still unclear, some connections of radio halos and relics with dynamical motion of ICM are reported. GeV electrons in radio halos and relics are expected to emit non-thermal hard X-ray via inverse Compton process of CMB photons. Comparing the synchrotron radio flux and inverse Compton hard X-ray one (or its upper limit), we are able to estimate volume-averaged magnetic field strength (or its lower limit).

Hard X-ray Properties

- Hard X-ray emission from A2319 is clearly detected in the energy below ~ 40 keV
- PIN alone spectrum is better represented by a thermal model.



PIN spectrum

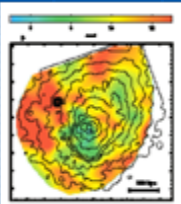
Black: data
Red: NXB model
Green: (data-NXB)
Blue: CXB model

Fitting results of the PIN spectrum

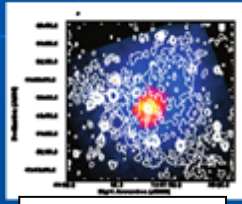
model	Γ or kT (keV)	$\chi^2/d.o.f$
PL	$3.1^{+0.1}_{-0.1}$	81.7/69
1kT	$10.9^{+0.9}_{-0.9}$	67.7/69

Abell 2319 Cluster

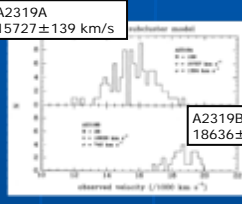
- Ra: 19h21m12s Dec: 43° 56m45s, z=0.0557
- Nearby well-known merging cluster with a radio halo
- Inhomogeneous temperature structures and a cold front found by Chandra
- Two subgroups are found in radial velocity distribution of the member galaxies.



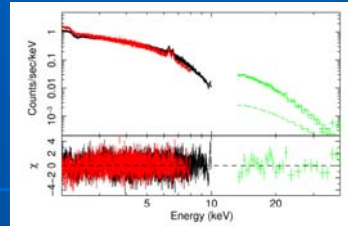
Chandra X-ray image and temperature map (Govoni et al. 2004)



ROSAT X-ray image (colors) and radio image (contours) (Feretti et al. 1997)



Line-of-sight velocity distribution of the member galaxies (Oegerle et al. 1995)



Wide band spectrum fitted with APEC+Powerlaw model

Black: XIS FI
Red: XIS BI
Green: PIN

- No significant power-law components
- Possible very hot (~ 16 keV) component

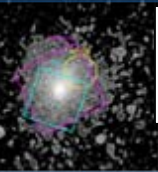
Fitting results of the XIS+PIN spectrum

	1kT	2kT
kT_{low} (keV)	$9.7^{+0.1}_{-0.1}$	$6.5^{+0.5}_{-0.5}$
kT_{high} (keV)	-	$15.7^{+1.2}_{-1.0}$
$Z(Z_{\odot})$	$0.26^{+0.01}_{-0.01}$	$0.28^{+0.01}_{-0.01}$
$N_{\text{H, XIS}}$	$0.17^{+0.00}_{-0.00}$	$8.5^{+1.1}_{-1.1} \times 10^{-2}$
$N_{\text{H, PIN}}$	$0.18^{+0.01}_{-0.01}$	$0.14^{+0.04}_{-0.04}$
$N_{\text{H, XIS+PIN}}$	-	$9.2^{+1.1}_{-1.2} \times 10^{-2}$
$N_{\text{H, PIN}}$	-	$6.4^{+1.4}_{-1.3} \times 10^{-2}$
$\chi^2/d.o.f.$	3215.6/2978	3136.6/2975

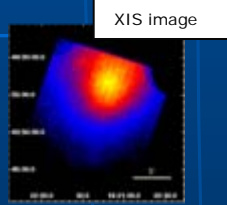
	1kT + PL(1.92)	1kT + PL(2.4)
kT_{low} (keV)	$9.7^{+0.1}_{-0.1}$	$9.7^{+0.1}_{-0.1}$
$Z(Z_{\odot})$	$0.26^{+0.01}_{-0.01}$	$0.26^{+0.01}_{-0.01}$
$N_{\text{H, XIS}}$	$0.17^{+0.00}_{-0.00}$	$0.17^{+0.00}_{-0.00}$
$N_{\text{H, PIN}}$	$0.16^{+0.02}_{-0.01}$	$0.15^{+0.02}_{-0.02}$
Γ_{PL}	1.92(fixed)	2.4(fixed)
N_{PLXIS}	$0.0^{+0.3}_{-0.0} \times 10^{-3}$	$0.0^{+0.3}_{-0.0} \times 10^{-3}$
N_{PLPIN}	$3.8^{+2.4}_{-1.7} \times 10^{-3}$	$2.2^{+1.4}_{-1.7} \times 10^{-2}$
$\chi^2/d.o.f.$	3210.9/2976	3211.2/2976

Observation

- 2006 October 27-30
- Exposure time: XIS 99.5 ks, HXD PIN 94.0 ks
- SCI-on, HXD nominal pointing



ROSAT image overlaid with XIS (blue) and HXD PIN FWHM (magenta) FOV, and A2319b (yellow).



XIS image

Constraint of Non-thermal Components and Magnetic Field Strength

- The upper limit of the power-law component flux and lower limit of the magnetic field strength become $\sim 3 \times 10^{-11}$ erg s⁻¹ cm⁻² and ~ 0.2 μ G, respectively, though the results slightly depend on the detailed spectral modeling.

Flux of a power-law component in 10-40 keV and its upper limits

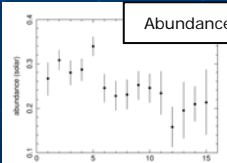
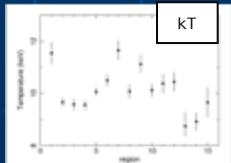
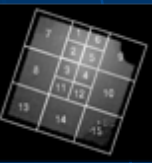
model	flux (erg s ⁻¹ cm ⁻²)	upper limit (erg s ⁻¹ cm ⁻²)
1kT + PL(1.92)	$1.1^{+0.8+1.1}_{-0.8-1.1} \times 10^{-11}$	$< 2.6 \times 10^{-11}$
1kT + PL(2.4)	$1.5^{+1.3+1.9}_{-0.8-1.2} \times 10^{-11}$	$< 3.8 \times 10^{-11}$
2kT + PL(1.92)	$0.0^{+2.7+3.2}_{-0.0-0.0} \times 10^{-11}$	$< 4.3 \times 10^{-11}$
2kT + PL(2.4)	$0.0^{+5.2+5.8}_{-0.0-0.0} \times 10^{-11}$	$< 4.5 \times 10^{-11}$

The lower limit of the magnetic field strength

model	$B(\mu\text{G})$
1kT + PL(1.92)	> 0.19
1kT + PL(2.4)	> 0.27
2kT + PL(1.92)	> 0.14
2kT + PL(2.4)	> 0.25

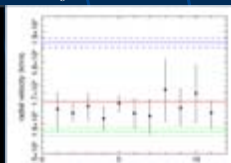
Temperature and Abundance Structures

- The central south-east regions (region 2, 3, 4) tend to have lower temperature, and higher abundance. These regions are just in the north-west of the cold front.



Line-of-sight Velocities of the ICM

- It is clear that the observed velocities are different than that of A2319B subgroup.
- No significant velocity difference is detected within the observed region.
- $\Delta v < 940^{+1083}_{-1131}$ km/s. (cf. $c_s \sim 1700$ km/s)



Line-of-sight velocity

Blue: A2319B subgroup
Green: A2319A subgroup
Red: A2319

Summary

- ◆ We observed the central region of the Abell 2319 with Suzaku.
- ◆ We found for the first time that the central cool region in the north-west of the cold front has higher metal abundance.
- ◆ The line-of-sight velocities in the observed region are clearly different than that of A2319b subgroup.
- ◆ No significant velocity difference is detected within the observed region, which means that the ICM motion is probably subsonic.
- ◆ The upper limit of the power-law component flux and lower limit of the magnetic field strength become $\sim 3 \times 10^{-11}$ erg s⁻¹ cm⁻² and ~ 0.2 μ G, respectively, though the results slightly depend on the detailed spectral modeling.
- ◆ Considering the lack of a significant amount of very hot (~ 20 keV) gas and the strong bulk flow motion, it is more likely that the relativistic non-thermal electrons are accelerated through the intracluster turbulence rather than the shocks.

(References)

- Feretti et al. 1997, NewA, 2, 501
- Govoni et al. 2004, ApJ, 605, 695
- Oegerle et al. 1995, AJ, 110, 32
- Sugawara et al. 2009, submitted to PASJ